

# Multiwavelength modelling the SED of supersoft X-ray sources

## III. RS Ophiuchi: The supersoft X-ray phase and beyond

A. Skopal,<sup>1,2</sup>

*Astronomical Institute, Slovak Academy of Sciences, 059 60 Tatranská Lomnica, Slovakia*

Received 17 July 2013; accepted 20 May 2014

### HIGHLIGHTS

- Multiwavelength model SEDs of the nova RS Oph from X-rays to mid-IR were performed.
- During the supersoft source phase its luminosity was highly super-Eddington.
- It was sustained by a high accretion rate from a disk, followed by jets.
- During quiescence the SED satisfied radiation produced by a large accretion disk.
- The high accretion rate could be realized throughout a focused wind of the giant.

### Abstract

I modelled the 14 Å–37 μm SED of the recurrent symbiotic nova RS Oph during its supersoft source (SSS) phase and the following quiescent phase. During the SSS phase, the model SEDs revealed the presence of a strong stellar and nebular component of radiation in the spectrum. The former was emitted by the burning WD at highly super-Eddington rate, while the latter represented a fraction of its radiation reprocessed by the thermal nebula. During the transition phase, both the components were decreasing and during quiescence the SED satisfied radiation produced by a large, optically thick disk ( $R_{\text{disk}} > 10 R_{\odot}$ ). The super-Eddington luminosity of the burning WD during the SSS phase was independently justified by the high quantity of the nebular emission. The emitting material surrounded the burning WD, and its mass was  $(1.6 \pm 0.5) \times 10^{-4} (d/1.6 \text{ kpc})^{5/2} M_{\odot}$ . The helium ash, deposited on the WD surface during the whole burning period, was around of  $8 \times 10^{-6} (d/1.6 \text{ kpc})^2 M_{\odot}$ , which yields an average growing rate of the WD mass,  $\dot{M}_{\text{WD}} \sim 4 \times 10^{-7} (d/1.6 \text{ kpc})^2 M_{\odot} \text{ yr}^{-1}$ . The mass accreted by the WD between outbursts,  $m_{\text{acc}} \sim 1.26 \times 10^{-5} M_{\odot}$ , constrains the average accretion rate,  $\dot{M}_{\text{acc}} \sim 6.3 \times 10^{-7} M_{\odot} \text{ yr}^{-1}$ . During quiescence, the accretion rate from the model SED of  $\sim 2.3 \times 10^{-7} M_{\odot} \text{ yr}^{-1}$  requires a super-Eddington accretion from the disk at  $\sim 3.6 \times 10^{-5} M_{\odot} \text{ yr}^{-1}$  during the outburst. Such a high accretion can be responsible for the super-Eddington luminosity during the whole burning phase. Simultaneous presence of jets supports this scenario. If the wind from the giant is not sufficient to feed the WD at the required rate, the accretion can be realized from the disk-like reservoir of material around the WD. In this case the time between outbursts will extend, with the next explosion beyond 2027. In the opposite case, the wind from the giant has to be focused to the orbital plane to sustain the high accretion rate at a few  $\times 10^{-7} M_{\odot} \text{ yr}^{-1}$ . Then the next explosion can occur even prior to 2027.

*Key words:* Stars: fundamental parameters – individual: RS Oph – binaries: symbiotic – novae, cataclysmic variables – X-rays: binaries

### 1. Introduction

The last outburst of the recurrent symbiotic nova RS Oph was discovered by Narumi et al. (2006) on 2006 February 12.83 UT. Due to its expectation and a bright peak magnitude of  $V = 4.5$ , a large amount of observations at different dates of the nova evolution, throughout a very wide wavelength range was carried out by telescopes from the ground and onboard the satellites (e.g. Evans et al. , 2007, and references therein). During the first 30 days after the eruption, observations indicated a non-spherical shaping of the nova ejecta (e.g. O’Brien et al. , 2006, in the radio). The multiwavelength modelling the SED from this period revealed a biconical ionization structure of the nova that developed during the first four days and that the luminosity was well above the Eddington limit (Skopal , 2015b, (Paper II)). Signatures of the blast wave produced in the nova explosion were detected by the *Swift* and *RXTE* satel-

lites in the form of a strong 0.5–20 keV X-rays (Bode et al. , 2006; Sokoloski et al. , 2006). The authors interpreted the behaviour of the hard X-ray flux as a result of the evolution of shock systems due to the impact of high-velocity ejecta into the red giant wind.

Around day 26, a luminous and highly variable supersoft X-ray component began to appear in the spectrum (Bode et al. , 2006; Ness et al. , 2009; Osborne et al. , 2011). RS Oph thus entered its SSS phase, which lasted to about day 90 (Osborne et al. , 2006). Between days 40 and 80 the supersoft X-ray fluxes were relatively stable (Hachisu et al. , 2007; Osborne et al. , 2011). This period of the nova evolution provides a good occasion to determine the fundamental parameters of the burning WD, because of the possibility to measure its radiation throughout a broad energy region.

Ness et al. (2007) analyzed first the X-ray *Chandra* and *XMM-Newton* grating spectra from the SSS phase. On day 54, they found the best agreement between their blackbody models and observations for the temperature and luminosity  $T \sim (520 - 580) \times 10^3 \text{ K}$  and  $\log(L) = 39.3 - 40.0$ ,

<sup>1</sup> E-mail: skopal@ta3.sk

<sup>2</sup> Visiting Astronomer: Astronomical Institut, Bamberg

<sup>3</sup> <http://dx.doi.org/10.1016/j.newast.2014.05.008>

respectively, however without specifying the corresponding  $N_{\text{H}}$ . They did not claim from these models that a super-Eddington luminosity occurred.

Nelson et al. (2008) compared this spectrum with WD atmospheric models, and selected that with  $T \sim 820000 \pm 10000$  K and  $N_{\text{H}} = 2.3 \times 10^{21} \text{ cm}^{-2}$  for  $L \equiv L_{\text{Edd}}$ .

Osborne et al. (2011) performed spectral fits to the *Swift*-XRT SSS spectra by the atmosphere models. They obtained  $kT \sim 90$  eV ( $\sim 1.04 \times 10^6$  K),  $R \sim 4 \times 10^8$  cm ( $\sim 0.0057 R_{\odot}$ ) and  $L \sim 3 \times 10^4 L_{\odot}$ .

The very different quantities of fundamental parameters of the burning WD during the SSS phase, as derived by different groups of authors, result probably from the problem of mutual dependence between the parameters  $L$ ,  $N_{\text{H}}$ ,  $T$  in fitting only the X-ray data (see Sect. 4 of Skopal, 2015a, Paper I therein).

In this contribution I aim to determine the fundamental ( $L$ ,  $R$ ,  $T$ ) and  $N_{\text{H}}$  parameters of the global spectrum produced by RS Oph during the SSS phase and beyond it by modelling its SED throughout the very large spectral range, 0.0014–37  $\mu\text{m}$ . Section 2 introduces multiwavelength observations at selected days, the results of their SED-fitting analysis are given in Sect. 3, and discussion with summary are found in Sects. 4 and 5, respectively.

## 2. Observations

As in the Paper II (see Sect. 2 there) I used observations obtained during the two recent, 1985 and 2006, outbursts. I complemented the X-ray observations from the SSS phase of the 2006 outburst with the nearest (in days after the maximum) *IUE* spectra, the optical  $UBVR_{CI}$  and the infrared  $JHKL$  photometric flux-points from the 1985 outburst, and with those obtained by the Infrared Spectrometer on the *Spitzer Space Telescope* (Evans et al., 2007, DDT, PID 270). Photometric measurements were interpolated to dates of the *IUE* spectra with the aid of light curves (LC) published by Evans et al. (1988).

For the SSS phase, I analyzed three X-ray spectra obtained with *Chandra* (day 40 and 67) and *XMM-Newton* (day 54), i.e. close to the beginning, middle and the end of the stable SSS phase. These X-ray spectra were already analyzed by Ness et al. (2007), Nelson et al. (2008) and Ness et al. (2009), who also provided their detailed description and treatment. For the aim of this paper I selected around 20 representative fluxes from the figure 4 of Ness et al. (2007).

Beyond the SSS phase, during the monotonic decline following the plateau phase (day  $\gtrsim 80$ ), two *IUE* spectra were exposed on day 93.6 (SWP25815/LWP05865) and 106.1 (SWP25920/LWP05962). They were complemented with the photometric  $V$  and  $I_C$  flux-points. Other photometric fluxes could not be used to estimate the true continuum, because of saturation by a strong emission line spectrum. During the post-outburst minimum (Fig. 1), the UV/optical SED was determined from the *IUE* spectra

Table 1  
Log of observations

Date	Julian date	Day <sup>a</sup>	Region	Observatory
Mar 15, 2006	2 453819.08	39.76	1.40–3.40 nm	<i>Chandra</i>
Mar 1, 1985	2 446134.70	42.73	115–335 nm	<i>IUE</i>
Mar 1, 1985	2 446134.70	42.73	<i>UVIC JHKL</i>	<i>SAAO</i> <sup>b</sup>
Mar 29, 2006	2 453833.49	54.16	1.50–3.3 nm	<i>XMM-Newton</i>
Mar 14, 1985	2 446147.76	54.79	115–335 nm	<i>IUE</i>
Mar 14, 1985	2 446147.76	54.79	<i>UVIC JHKL</i>	<i>SAAO</i> <sup>b</sup>
Apr 7, 2006	2 453841.84	62.51	5.28–37.1 $\mu\text{m}$	<i>Spitzer</i>
Apr 11, 2006	2 453846.29	66.96	1.50–3.20 nm	<i>Chandra</i>
Mar 31, 1985	2 446164.63	72.66	115–335 nm	<i>IUE</i>
Mar 31, 1985	2 446164.63	72.66	<i>UVIC JHKL</i>	<i>SAAO</i> <sup>b</sup>
Apr 17, 2006	2 453851.87	72.54	5.28–37.1 $\mu\text{m}$	<i>Spitzer</i>
Apr 21, 1985	2 446185.61	93.64	115–335 nm	<i>IUE</i>
May 3, 1985	2 446198.07	106.1	115–335 nm	<i>IUE</i>
Sep 27, 1985	2 446345.25	253.3	115–335 nm	<i>IUE</i>
Sep 23, 1986	2 446706.14	614.2	115–335 nm	<i>IUE</i>

<sup>a</sup> = JD – JD<sub>max</sub> (JD<sub>max</sub> 2 446 091.97 as on 1985 Jan. 26.47;  
JD<sub>max</sub> 2 453 779.33 as on 2006 Feb. 12.83)

<sup>b</sup> values from Evans et al. (1988) interpolated to JD(*IUE*)

SWP26883/LWP06860 from 06/10/1985 (day 253.3) and the flux corresponding to the visual magnitude  $12.0 \pm 0.5$ . The short-wavelength part of the LWP spectrum (2000–2400 Å) was underexposed and thus not used to model the SED (dotted line in Fig. 3). During the quiescent phase of RS Oph, which was established about 1 year after the outbursts, the SED was determined from the *IUE* spectrum SWP29351/LWP09232 from 02/10/1986 (day 614.2),  $UBVR_{CI}$  and  $JHKL$  photometric fluxes from 30/09/1986 and 26/09/1986, respectively (Evans et al., 1988).

Evolution in the optical brightness of the 2006 outburst, the period of its stable SSS phase and timing of the used spectroscopic observations are shown in Fig. 1. In modelling the data I used the same absorption model, colour excess and distance to RS Oph as in the Paper II. The log of the used observations is given in Table 1.

## 3. Results of the SED-fitting analysis

### 3.1. Modelling the SED during the SSS phase

I performed the the SED-fitting analysis in the same way as described in the section 2.6 of Paper I. In addition, the observed grating spectra show a variable, but pronounced, jump absorption at  $\sim 23.5$  Å, which is due to the oxygen absorption edge. According to Ness et al. (2007), changes in the O I absorption edge profile at different days are caused by a different abundance of O I atoms within the material in the line of sight. Therefore, to minimize the  $\chi^2$  sum, I

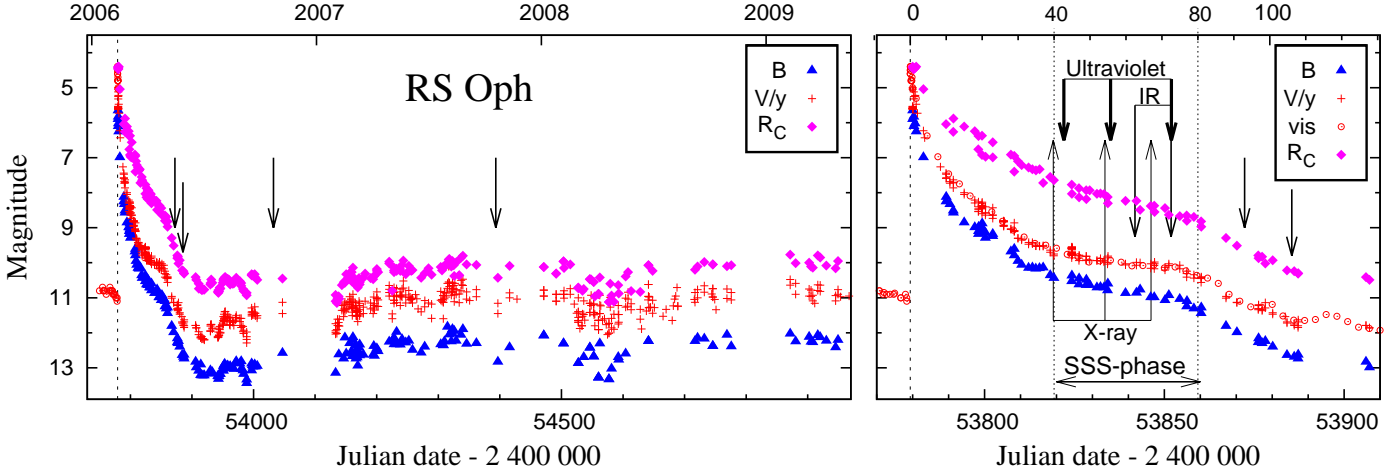


Fig. 1. The  $BVR_C$  LCs of RS Oph from the maximum at 2006 February 12.83 (vertical dashed lines). The data were collected by the VSOLJ observers, Kiyota, Kubotera, Maehara and Nakajima. Visual estimates are from CDS. The right panel shows a detail covering the 2006 outburst. The plateau phase between day 40 and 80 coincides with a stable SSS phase of the nova evolution. Vertical arrows denote timing of the used spectroscopic observations (Table 1).

Table 2

Parameters of the X-ray—IR SED-fitting analysis (Sect. 3, Figs. 2 and 3)

Day	$\xi$	$N_H$ [ $10^{21} \text{ cm}^{-2}$ ]	$T_h$ [kK]	$\theta_h/10^{-12}$	$R_h^{\text{eff}}$ [ $R_\odot$ ]	$\log(L_h)$ [ $\text{erg s}^{-1}$ ]	$L_{\text{ph}}(\text{H})$ [ $\text{s}^{-1}$ ]	$T_e$ [K]	$EM$ [ $\text{cm}^{-3}$ ]	$\chi_{\text{red}}^2$ / d.o.f.
40*	$\sim 0.25$	$7.3 \pm 0.2$	$460 \pm 10$	$3.9 \pm 0.7$	$0.28 \pm 0.04$	$40.08 \pm 0.13$	$6.8 \times 10^{49}$	36,000	$3.4 \times 10^{61}$	5.9 / 38
54*	$\sim 0.6$	$6.8 \pm 0.3$	$495 \pm 20$	$3.0 \pm 0.6$	$0.21 \pm 0.05$	$39.98 \pm 0.18$	$5.0 \times 10^{49}$	29,000	$2.2 \times 10^{61}$	4.9 / 42
67*	$\sim 0.4$	$7.0 \pm 0.2$	$505 \pm 10$	$2.7 \pm 0.5$	$0.19 \pm 0.03$	$39.91 \pm 0.11$	$4.3 \times 10^{49}$	26,000	$9.8 \times 10^{60}$	5.5 / 38
93 <sup>†</sup>			$> 90^a$	$< 4.0$	$< 0.29$	$> 37.27$	$> 3.6 \times 10^{47}$	17000	$2.2 \times 10^{60}$	1.2 / 11
106 <sup>†</sup>			$> 100^a$	$< 2.7$	$< 0.19$	$> 37.10$	$> 2.4 \times 10^{47}$	19000	$1.7 \times 10^{60}$	1.5 / 11
253 <sup>†</sup>			$25 \pm 2$	$14.5 \pm 1.5$	$1.0 \pm 0.1$	$36.14 \pm 0.13$	$6.3 \sim 10^{46}$	27000	$\lesssim 10^{59}$	0.9 / 10
614 <sup>†, b</sup>			$17.2^c$	$130 \pm 15$	$9.4 \pm 0.9^d$	$36.16 \pm 0.13^e$				3.6 / 13

\* according to the timing of the X-ray observations, <sup>†</sup> according to the timing of the *IUE* observations, <sup>a</sup> =  $T_h^{\text{min}}$  (Sect. 3.2), <sup>b</sup> accretion disk (AD) model, <sup>c</sup> =  $T_{\text{disk}}^{\text{max}}$  of the AD-model, <sup>d</sup> i.e.  $R_{\text{disk}} > 10 R_\odot$ , <sup>e</sup> =  $L(\text{AD})/\cos(i)$ .

reduced the optical depth in the line of sight by a fractional contribution from oxygen, i.e. using  $\tau_x = \sigma_x N_H = (\sigma_{\text{ISM}} - \xi \sigma_{\text{OI}}) N_H$  in Eq. (3) of Paper I, where  $\sigma_{\text{OI}}$  is the O I cross section in the ISM model reduced with a factor  $0 < \xi < 1$ . This factor thus represents an additional fitting parameter. Then, assuming that the interstellar part of the optical depth ( $N_H(\text{ISM})\sigma_{\text{ISM}}$ ) persists as a constant, one can derive the abundance of the oxygen content within the *circumstellar* material in the line of sight as

$$A_{\text{OI}}(\text{CSM}) = A_{\text{OI}}(\text{ISM}) \left( 1 - \xi \frac{N_H}{N_H(\text{CSM})} \right), \quad (1)$$

where the oxygen abundance in the ISM,  $A_{\text{OI}}(\text{ISM}) = 0.00049$  (Wilms et al., 2000), and the hydrogen column density within the circumstellar matter,  $N_H(\text{CSM}) = N_H - N_H(\text{ISM})$ , as given by Eq. (4) of Paper I.

For day 40 I fitted 18 X-ray fluxes from 14 to 32 Å, 19 UV fluxes between 1170 and 3300 Å and the photometric *UVI*<sub>C</sub>*JHKL* flux-points. I omitted flux-points derived from the *B* and *R<sub>C</sub>* photometric measurements, because of a significant effect of emission lines in these passbands (see Skopal, 2007). The best-fit-model and the flux-point

errors yielded the reduced  $\chi_{\text{red}}^2 = 5.9$  for 38 degrees of freedom. The larger value of  $\chi_{\text{red}}^2$  results mainly from small and thus uncertain fluxes from the short-wavelength part of the spectrum with the fixed 10% errors only. In the same way I reconstructed the composite X-ray—IR continuum at days 54–55 and 67–73. All solutions required the total  $N_H > N_H(\text{ISM})$  that reflects a significant contribution to b-f absorptions by the CSM during the SSS phase of RS Oph (Table 2).

On day 40, the best-fit-model of the SSS suggested a reduction of the O I content in the line of sight by  $\sim 25\%$  ( $\xi \sim 0.25$ ), i.e. by  $\sim 37\%$  ( $= 0.25 N_H / N_H(\text{CSM}) \times 100\%$ ) within the circumstellar matter. On day 54, the best fit suggested the parameter  $\xi \sim 0.6$ , which reduces oxygen within the CSM by more than 90%. However, on day 67 the oxygen abundance  $A_{\text{OI}}(\text{CSM})$  increased to  $\sim 0.4 A_{\text{OI}}(\text{ISM})$ . Similar results were found also by Ness et al. (2007).

The *Spitzer* spectra could not be used in the fitting procedure, because they were not taken simultaneously with other modelled fluxes. Nevertheless, by multiplying them with an appropriate constant, the slope of their continuum followed that of the nebular component of radiation, which

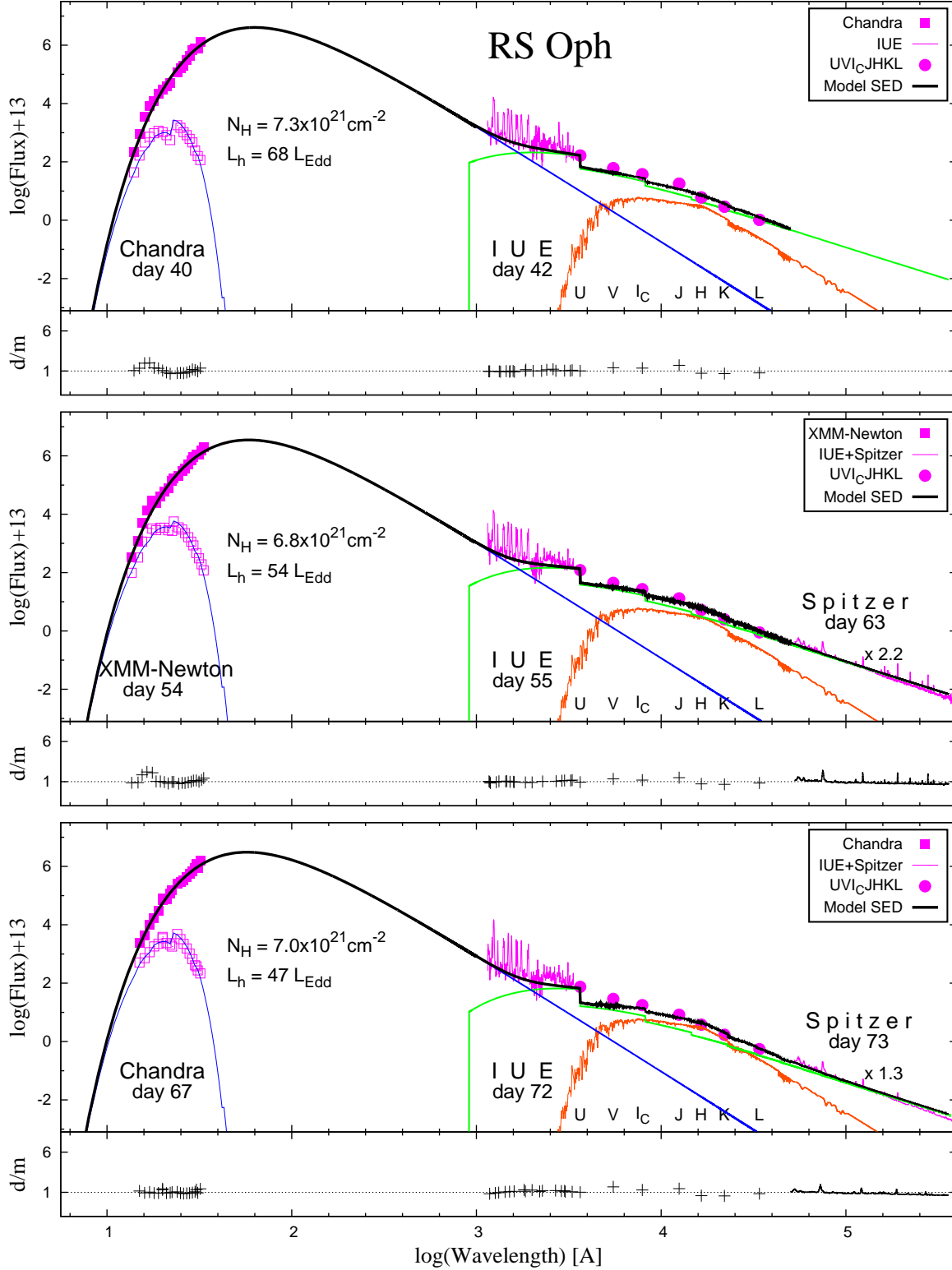


Fig. 2. A comparison of the observed (in violet) and model (heavy black line) SED of RS Oph during its supersoft source phase with corresponding data-to-model ratios ( $d/m$ ). Open/filled squares are the absorbed/unabsorbed X-ray fluxes. Fluxes are in units of  $\text{erg cm}^{-2} \text{s}^{-1} \text{\AA}^{-1}$ . The blue, green and orange line denotes the component of radiation from the WD, nebula and giant, respectively.

dominates the mid-IR domain (see Fig. 2). Thus the SED-fitting analysis proved independently the nebular origin of the *Spitzer* spectra as suggested by Evans et al. (2007).

I made a rough estimate of the uncertainties in  $T_h$  and  $N_H$  by comparing more models around the best solution. All models with different  $T_h$  and  $N_H$  were scaled to the dereddened far-UV fluxes. In this way I estimated  $\Delta T_h \sim$

10000 – 20000 K and  $\Delta N_{\text{H}} \sim 0.2 - 0.3 \times 10^{21} \text{ cm}^{-2}$ . The uncertainty for  $\theta_{\text{h}}$  was then derived with the aid of Eq. (6) of Paper I as the mean error of the  $\theta_{\text{h}}(N_{\text{H}}, T_{\text{h}})$  total differential. Similarly, I derived the uncertainty in  $L_{\text{h}}$  as a function of  $R_{\text{h}}$  and  $T_{\text{h}}$  in the Stefan-Boltzman law.

### 3.2. Modelling the SED beyond the SSS phase

The model SED during the monotonic decline following the plateau phase (day 93.6 and 106.1) showed a significant decrease of both the stellar and the nebular component of radiation. Having only the UV part of the total WD spectrum, it was possible to determine only the minimum temperature,  $T_{\text{h}}^{\text{min}} = 0.9 - 1 \times 10^5 \text{ K}$ , at which the WD’s radiation gives rise to the observed *EM* and fits the far-UV fluxes (see Appendix A of Paper II). The *EM* of the nebula decreased by a factor of  $\sim 5$  with respect to the day 67, but still dominated the optical.

During the post-outburst minimum (day 253) the WD became significantly cooler, radiating at  $\sim 25000 \text{ K}$  and having an angular radius  $\theta_{\text{h}} \sim 1.45 \times 10^{-11}$  (i.e.  $R_{\text{h}} \sim 1.03(d/1.6 \text{ kpc}) R_{\odot}$  and  $L_{\text{h}} \sim 370(d/1.6 \text{ kpc})^2 L_{\odot}$ ). The nebular emission was negligible with respect to contributions from the giant and WD (Fig. 3).

During the quiescent phase (day 614) the SED profile throughout the UV/optical was more or less flat with the optical fluxes well above the radiation from the giant. A simple blackbody radiation could in no way match the flat SED, particularly not the optical (see Fig. 3, dashed line). Accordingly, I performed its modelling with a function,

$$F_{\text{h}}^{\text{obs}}(\lambda) = \theta_{\text{h}}^2 (F_{\lambda}(\text{AD}) + 0.6\pi B_{\lambda}(T_{\text{BL}})), \quad (2)$$

where the first term at the right represents the flux distribution of an optically thick accretion disk that radiates locally like a black body, while the second term is a contribution from the boundary layer radiating at a temperature  $T_{\text{BL}}$ . The disk temperature  $T_{\star} = 2T_{\text{disk}}^{\text{max}}$  determines the slope of the UV continuum (see e.g. Warner, 1995, in detail). The observed flat UV continuum corresponds to  $T_{\text{disk}}^{\text{max}} = 17200 \text{ K}$ ,  $T_{\text{BL}} \sim 79000 \text{ K}$  and  $\theta_{\text{h}} = 1.3 \times 10^{-10}$ . These parameters yield an effective (spherical) radius  $R_{\text{h}}^{\text{eff}} \sim 9.4(d/1.6 \text{ kpc}) R_{\odot}$ , suggesting that the linear radius of the disk  $R_{\text{disk}} > 10 R_{\odot}$ . The luminosity of the disk from the model SED is  $L_{\text{disk}} \sim 380/\cos(i) L_{\odot}$  and its boundary layer  $L_{\text{BL}} \sim 700 L_{\odot}$ . However, the boundary layer is not well defined by the observed SED, because the far-UV fluxes are very uncertain. For example, their steepness could be simulated by an iron curtain absorption at longer wavelengths.

The model SEDs are depicted in Figs. 2 and 3 and corresponding physical parameters are found in Table 2.

## 4. Interpretation of observations

The model SEDs throughout the  $14 \text{ \AA} - 37 \mu\text{m}$  range identified a strong *stellar* and *nebular* component of radiation

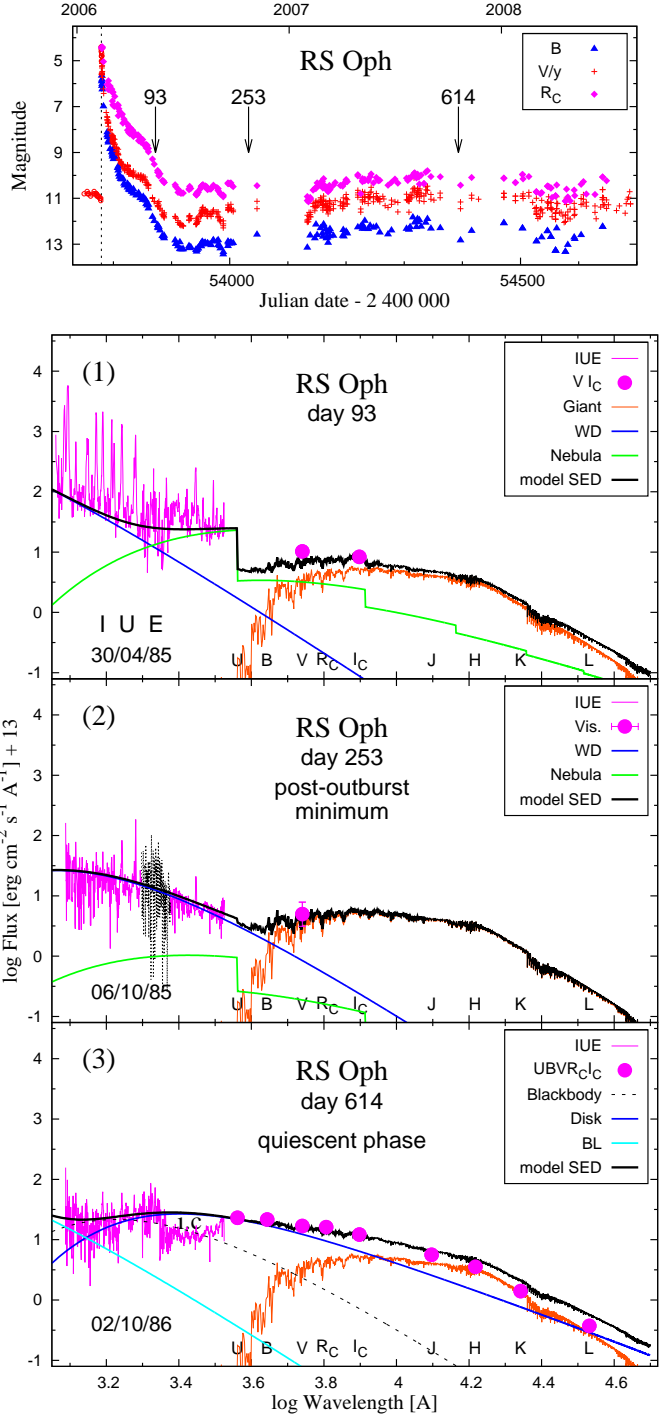


Fig. 3. Model SEDs beyond the SSS phase. (1) During the decline following the plateau phase (day 93), (2) during the post-outburst minimum (day 253) and (3) during the quiescence (day 614). Their timing is denoted by arrows in the top panel with the LC. Denotation of lines as in Fig. 2. The dashed line in the bottom panel shows a Planck curve for a comparison (see Sect. 3.2). A depression of the UV continuum due to the iron curtain absorption is denoted by ‘i.c.’.

in the spectrum of RS Oph. The former is produced by the WD photosphere and dominates the spectrum from the X-rays to the far-UV, whereas the latter represents its fraction reprocessed by a thermal nebula via the  $b-f/(f-b)$  and  $f-f$

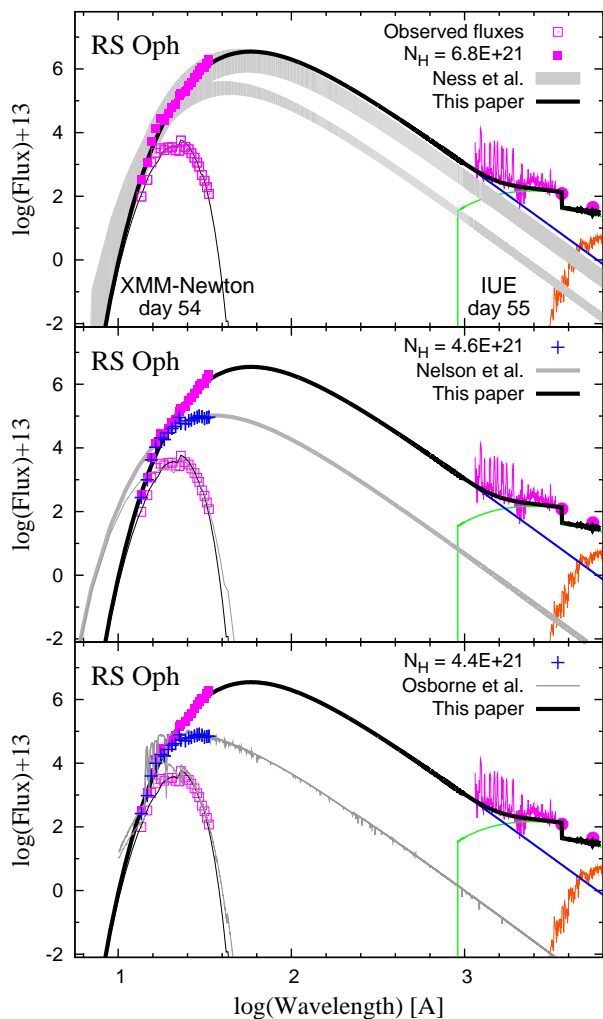


Fig. 4. Comparison of the multiwavelength model SED from day 54 (Fig. 2) and the X-ray-data models of Ness et al. (2007) (top), Nelson et al. (2008) (middle) and Osborne et al. (2011) (bottom).

transitions under conditions of Case B. The nebula dominates the spectrum for  $\lambda \gtrsim 2000 \text{ \AA}$  (Fig. 2). However, the corresponding physical parameters are very different from those inferred from modelling only the X-ray data.

#### 4.1. Comparison with previous models

Ness et al. (2007) first analyzed the grating spectra of RS Oph obtained by *Chandra* and *XMM-Newton* during the SSS phase (Sect. 2). They developed a series of blackbody models to match the continuum emission, and found reasonable agreement with the measured spectra. The top panel of Fig. 4 compares their models with that of this paper for day 54. The authors found the temperature and luminosity to be in the range of  $T_h = (650 - 710) \times 10^3 \text{ K}$  and  $\log(L_h) = 38.5 - 38.9$ , respectively, for  $N_H \sim 5.3 \times 10^{21} \text{ cm}^{-2}$  (the lower shadow belt in the figure). By varying the oxygen abundance in the CSM component, they obtained a better agreement with  $T_h = (520 - 580) \times 10^3 \text{ K}$ ,  $\log(L_h) = 39.3 - 40.0$  and  $N_H \sim 6.9 \times 10^{21} \text{ cm}^{-2}$  ( $N_H$  according to Ness, private communication). The latter series

of their models (see the upper shadow area in Fig. 4) is in a good agreement with the model of this paper. However, the authors did not claim from these models that a super-Eddington luminosity occurred. Because of modelling only the X-ray data, they were not able to decide on the reliability of their second sets of solutions.

Nelson et al. (2008) instead compared the observed spectra with atmospheric models calculated by Rauch (2003). As the best-fit model they selected that with  $T_h = 820000 \pm 10000 \text{ K}$  and  $N_H = 2.3 \times 10^{21} \text{ cm}^{-2}$  for the spectrum from day 54. Even fitting a blackbody to the spectra, they still obtained a temperature close to  $800000 \text{ K}$ . Also these authors assumed that the WD luminosity does not exceed the Eddington value. The middle panel of Fig. 4 shows that their blackbody model ( $T_h = 800000 \text{ K}$ ,  $L_h \equiv L_{\text{Edd}}$ ) is a factor of  $\sim 150$  below the observed far-UV spectrum. In spite of this inconsistency, the X-ray data can still match their model with  $N_H \sim 4.6 \times 10^{21} \text{ cm}^{-2}$  (Fig. 4).

Osborne et al. (2011) performed spectral fits to the *Swift*-XRT spectra by both the blackbody and the atmosphere models. Although their plateau blackbody and model atmosphere luminosities were the same, they preferred the parameters given by the atmosphere models. During the plateau phase, around a maximum ( $\sim$ day 54, see their Fig. 4), they obtained  $kT \sim 90 \text{ eV}$  ( $\sim 1.04 \times 10^6 \text{ K}$ ),  $R \sim 4 \times 10^8 \text{ cm}$  ( $\sim 0.0057 R_\odot$ ),  $L \sim 3 \times 10^4 L_\odot$ . They did not specify the corresponding  $N_H$ . To determine its value, they used a power-law decrease of its CSM component (according to Bode et al., 2006), which should result in the total  $N_H = 3.4 \times 10^{21} \text{ cm}^{-2}$  on day 54. The authors also pointed out the gratifying agreement between their luminosities and those predicted theoretically by Iben and Tutukov (1996) for the plateau phase in the nova evolution. The bottom panel of Fig. 4 shows an example of their atmospheric model (spectrum 1020000-9.00-HHeCNOeMgSiS made on 2010-09-09 and 2011-01-26, available at <sup>4</sup>), calculated for  $T_{\text{eff}} = 1.02 \times 10^6 \text{ K}$  and scaled to  $L_h = 2.5 \times 10^4 L_\odot$  in the figure. However, the *XMM-Newton* fluxes had to be de-absorbed with  $N_H \sim 4.4 \times 10^{21} \text{ cm}^{-2}$  to match the model. Also in this case, the X-ray-data fit is far below the UV fluxes.

In terms of the multiwavelength approach, the large differences between the parameters obtained by different groups of authors result from the well known mutual dependence between the parameters  $L_h$ ,  $N_H$  and  $T_h$  in fitting only the X-ray data: a larger/lower  $L_h$  requires a larger/lower  $N_H$  and a lower/higher  $T_h$  to fit the absorbed X-ray fluxes (see Sect. 4.1 of Paper I).

#### 4.2. Are there other sources contributing to the far-UV ?

I consider the following two possibilities. (i) An accretion process at the super-Eddington rate of  $\sim 3.6 \times 10^{-5} M_\odot \text{ yr}^{-1}$  (see below, Sect. 4.7.3) can release in maximum its binding energy of  $\sim 1.4 \times 10^{39} \text{ erg s}^{-1}$

<sup>4</sup> <http://astro.uni-tuebingen.de/~rauch/VO/fluxtables/HHeCNOeMgSiS-gen/>

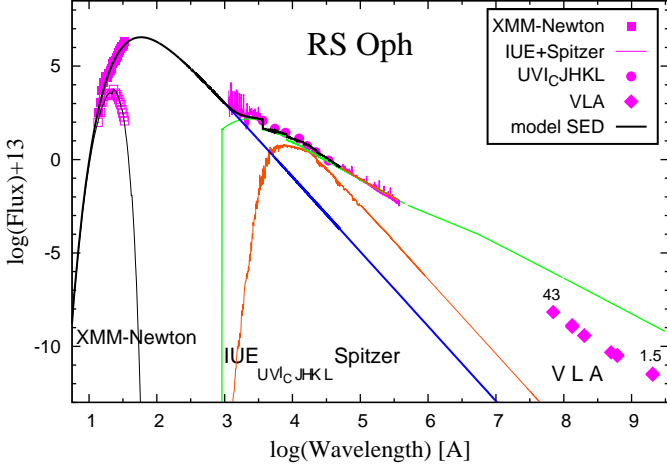


Fig. 5. The X-ray/radio SED for RS Oph around day 55. Denotation of lines is as in Fig. 2. Radio fluxes at 43, 22.5, 15, 6, 5 and 1.5 GHz were taken from Sokolowski et al. (2008) and Eyres et al. (2009). Their position shows that the nebula, which produces the UV/IR emission, is optically thick at radio frequencies (Sect. 4.3.1). The  $f - f$  Gaunt factor at radio frequencies was calculated according to approximation in Kwok (2000).

( $M_{\text{WD}} \sim 1.3 M_{\odot}$ ,  $R_{\text{WD}} \sim 0.004 R_{\odot}$ ; Sect. 4.6). The corresponding disk's luminosity is about twice the Eddington value. Its far-UV fluxes are well below the observed fluxes. (ii) The inverse Compton scattering of low energy photons off relativistic electrons cannot take place, because the plasma surrounding accreting WDs in the symbiotic novae and classical symbiotic stars contains non-relativistic electrons, as is clear from the presence of Thomson scattering measured in the strongest emission lines (e.g. O VI 1032 and 1038 Å doublet, see Sekeráš and Skopal, 2012).

If there is no other source, which contributes to the far-UV and rivals that from the burning WD, the very high far-UV fluxes ( $\sim 10^{-10} \text{ erg cm}^{-2} \text{ s}^{-1} \text{ Å}^{-1}$ , see Fig. 2) require the luminosity of the WD to be significantly above the Eddington limit. This can be probed independently by studying the very high emission from the thermal nebula.

#### 4.3. Relations between the stellar and nebular emission

The nebular emission represents a fraction of the stellar radiation from the WD reprocessed via the ionization/recombination and bremsstrahlung events. Therefore, its source can be associated with the material surrounding the burning WD.

The quantity of the nebular emission was determined by the model SED and its extent was revealed by direct imaging (O'Brien et al., 2006; Rupen et al., 2008; Sokolowski et al., 2008). At day 55, i.e. simultaneously with our second set of observations (Table 1), Sokolowski et al. (2008) observed RS Oph with the Very Large Array (VLA) at 43 GHz. They showed that the image emission is consistent with thermal bremsstrahlung emission from a lower temperature plasma heated by photoionizations. I used the im-

age and the corresponding flux to estimate the volume of the emitting material and its average particle density, and test whether these parameters are consistent with the high WD's luminosity suggested by the model SED.

##### 4.3.1. The emitting mass of the nebula

Here I assume that the emitting material that is imaged at 43 GHz produces the nebular radiation we measure at UV-IR wavelengths. First, approximating the shape of the VLA image by a prolate spheroid with an axis  $a \sim 34/\sin i \text{ mas} = 71(d/1.6 \text{ kpc}) \text{ AU}$  and  $b \sim 17.5 \text{ mas} = 28(d/1.6 \text{ kpc}) \text{ AU}$ , one obtains the volume of the main emission region,  $V^{\text{neb}} = 4/3\pi ab^2 \sim 7.8 \times 10^{44}(d/1.6 \text{ kpc})^3 \text{ cm}^3$ . The emission measure observed at day 55,  $EM = 2.2 \times 10^{61}(d/1.6 \text{ kpc})^2 \text{ cm}^{-3}$ , then yields an average particle density of this region,  $\bar{n} \sim 1.7 \times 10^8(d/1.6 \text{ kpc})^{-1/2} \text{ cm}^{-3}$ . These quantities correspond to an emitting mass of the nebula  $M^{\text{neb}} = \mu m_{\text{H}} \bar{n} V^{\text{neb}} \sim 1.6 \times 10^{-4}(d/1.6 \text{ kpc})^{5/2} M_{\odot}$ , where  $\mu \sim 1.4$  is the mean molecular weight and  $m_{\text{H}}$  is the mass of the hydrogen atom.

Second, using the measured flux at 43 GHz,  $F_{43} = 110 \pm 11 \text{ mJy}$  (Sokolowski et al., 2008), it is possible to verify results obtained from the image extension. Assuming that the plasma is optically thick at 43 GHz, and radiates under conditions of thermodynamical equilibrium, the nebula resembles a blackbody at temperature  $T_e$ . Then, using the Rayleigh-Jeans approximation ( $h\nu \ll kT_e$ , and no reddening applied), the angular radius of the nebula can be expressed as

$$\theta_{43} = \frac{c}{\nu} \left( \frac{\epsilon F_{43}}{2\pi k T_e} \right)^{1/2}, \quad (3)$$

where the filling factor  $\epsilon$  reduces the measured  $F_{43}$  flux to a value produced only by the optically thick part of the nebula at 43 GHz. Thus,  $\epsilon = 1$  yields a maximum effective radius of the nebula,  $R_{43}^{\text{eff}} = (7.2 \pm 0.4) \times 10^{14}(d/1.6 \text{ kpc}) \text{ cm}$ , which corresponds to a spherical volume,  $V_{43}^{\text{eff}} = (1.6 \pm 0.2) \times 10^{45}(d/1.6 \text{ kpc})^3 \text{ cm}^3$ . For  $\epsilon = 0.64$  both volumes are equal,  $V_{43}^{\text{eff}} = V^{\text{neb}}$ . Their comparability verifies the above adopted assumptions. The optical depth for such an extended and dense nebula is as large as a few hundred at 43 GHz (see Kwok, 2000, in detail). The optically thick case for the RS Oph remnant in the radio is demonstrated directly by the X-ray-radio SED (see Fig. 5). The radio fluxes are significantly lower than the nebular component of the radiation, which reproduces the UV-IR emission. So, if the measured  $EM$  corresponds to the  $V_{43}^{\text{eff}}$  volume, then  $\bar{n} = (1.2 \pm 0.1) \times 10^8(d/1.6 \text{ kpc})^{-1/2} \text{ cm}^{-3}$  and  $M_{43}^{\text{neb}} = (2.1 \pm 0.4) \times 10^{-4}(d/1.6 \text{ kpc})^{5/2} M_{\odot}$ .

Third, amount of the emitting mass can be proved independently by the hydrogen recombination lines, which are produced by the same volume of the nebula as the continuum. For example, using the  $H\alpha$ -line flux method (e.g. Gurzadyan, 1997; Kwok, 2000), the observed flux in the  $H\alpha$  line,  $F_{\alpha}$ , is produced by the ionized mass

$$M_{\alpha}^{neb} = 4\pi d^2 \frac{\mu m_{\text{H}}}{\varepsilon_{\alpha}(T_e) n_e} F_{\alpha}, \quad (4)$$

where  $\varepsilon_{\alpha}(T_e)$  is the volume emission coefficient in the H $\alpha$  line. Skopal et al. (2008) analyzed the profile of a strong H $\alpha$  line taken at day 57 (see their Fig. 3). According to Eq. (4), its integrated flux,  $F_{\alpha} = (6.5 \pm 0.1) \times 10^{-9} \text{ erg cm}^{-2} \text{ s}^{-1}$ , implies an emitting mass  $M_{\alpha}^{neb} = 1.1 - 1.6 \times 10^{-4} (d/1.6 \text{ kpc})^{5/2} M_{\odot}$  for  $n_e \equiv \bar{n} = 1.7 - 1.2 \times 10^8 (d/1.6 \text{ kpc})^{-1/2} \text{ cm}^{-3}$ , as derived above from the nebular continuum. The volume emission coefficient  $\varepsilon_{\alpha}(30000) = 1.24 \times 10^{-25} \text{ erg cm}^3 \text{ s}^{-1}$  (e.g. Osterbrock, 1989). The range of  $M_{\alpha}^{neb}$  values represents rather a lower limit, because the densest central part of the nebula, which contributes mainly to the line core, can be optically thick.

I conclude that: (i) the large quantity of  $EM$  derived from the SED, (ii) the volume and the flux of the emitting region measured by the VLA, and (iii) the strong flux in the H $\alpha$  line from the optical spectrum, all correspond to a high mass of the nebular emitting material,  $M^{neb} = (1.6 \pm 0.5) \times 10^{-4} (d/1.6 \text{ kpc})^{5/2} M_{\odot}$ , which surrounds the burning WD even during the SSS phase of its outbursts.

#### 4.3.2. Constraints for super-Eddington luminosity

(i) The nebular emission can be created only within the ionized part of the material surrounding the ionizing source. Its extent is limited by the distance from the WD's photosphere, at which the flux of its ionizing photons is balanced by the rate of ionization/recombination events inside the nebula. The radius of such an ionized zone is known as the Strömgen sphere,  $r_{\text{S}}$ . Here I express it in the form (see Eq. (3) of Skopal et al., 2009)

$$r_{\text{S}} = \left( \frac{3L_{\text{ph}}(\text{H})}{4\pi\alpha_{\text{B}}(\text{H}, T_e) \bar{n}^{-2}} \right)^{1/3}, \quad (5)$$

where  $L_{\text{ph}}(\text{H})$  is the flux of photons capable of ionizing hydrogen,  $\alpha_{\text{B}}(\text{H}, T_e)$  [ $\text{cm}^3 \text{ s}^{-1}$ ] stands for the total hydrogenic recombination coefficient in Case B, and  $\bar{n}$  is the mean particle density. The Eddington luminosity of the burning WD ( $44000 L_{\odot}$  for  $M_{\text{WD}} = 1.3 M_{\odot}$ ) radiating at  $8 - 10 \times 10^5 \text{ K}$  (Nelson et al., 2008; Osborne et al., 2011) corresponds to  $L_{\text{ph}}(\text{H}) = 5.6 - 4.5 \times 10^{47} \text{ s}^{-1}$ . Then  $\bar{n} = 1.7 \times 10^8 \text{ cm}^{-3}$  (Sect. 4.3.1) and  $\alpha_{\text{B}} = 1 \times 10^{-13} \text{ cm}^3 \text{ s}^{-1}$  yield  $r_{\text{S}} = 24 - 22 \text{ AU}$ , which is, however, smaller than the observed extent of the nebular material ( $a = 71$  and  $b = 28 \text{ AU}$ , Sect. 4.3.1). Thus, the WD radiating at the Eddington luminosity is not capable to ionize the observed volume of the material emitting at 43 GHz, whose image was used to determine  $\bar{n}$ . This implies that  $L_{\text{h}} > L_{\text{Edd}}$  to increase  $L_{\text{ph}}(\text{H})$  and thus  $r_{\text{S}}$ .

(ii) A lower limit of the WD luminosity can be estimated from the nebular component of radiation, which represents a fraction of the ionizing source radiation reprocessed by the thermal nebula via the ionization/recombination events. If *all* the ionizing photons are converted into the nebular radiation, then the *lower* limit of the WD luminosity, which

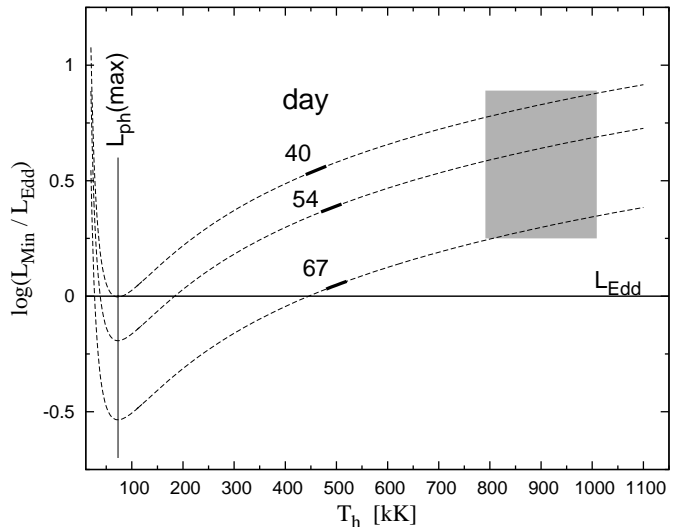


Fig. 6. The lower limit of the WD luminosity (Eq. (6)) as a function of its temperature scaled with  $EM$  as given by the model SED on day 40, 54 and 67. Solid thick bars bound ranges of  $T_{\text{h}}$  (Table 2). The gray belt denotes temperatures derived from the X-ray-data models (Nelson et al., 2008; Osborne et al., 2011). Vertical line points the minimum of the  $L_{\text{Min}}(T_{\text{h}})$  function at  $T_{\text{h}} = 73000 \text{ K}$ , for which the source produces a maximum flux of hydrogen ionizing photons,  $L_{\text{ph}}(\text{max})$  (see Sect. 4.3.2).

is capable of producing the observed  $EM$ , can be expressed as (see Appendix A of Paper II),

$$L_{\text{Min}}(T_{\text{h}}) = \alpha_{\text{B}}(\text{H}, T_e) EM \frac{\sigma T_{\text{h}}^4}{f(T_{\text{h}})}, \quad (6)$$

where the function

$$f(T_{\text{h}}) = \frac{\pi}{hc} \int_0^{912\text{\AA}} \lambda B_{\lambda}(T_{\text{h}}) d\lambda. \quad (7)$$

Equation (6) is valid for the hydrogen plasma, heated by photoionizations, and characterized with a constant  $T_e$  and  $\bar{n}$ . Thus, the  $EM$  constrains a minimum luminosity of the ionizing source as a function of its temperature. Figure 6 shows the  $L_{\text{Min}}(T_{\text{h}})$  function parameterized with the  $EM$  obtained from the model SED on day 40, 54 and 67. The minimum occurs at  $T_{\text{h}} \sim 73000 \text{ K}$ , at which the source produces a maximum  $L_{\text{ph}}(\text{H})$ . Higher values of  $L_{\text{Min}}(T_{\text{h}})$  on both sides reflect lower values of  $L_{\text{ph}}(\text{H})$ , which thus need a higher  $L_{\text{h}}(T_{\text{h}})$  of the source to give rise the measured  $EM$ . The steep increase of  $L_{\text{Min}}$  towards low  $T_{\text{h}}$  is due to a rapid decrease in  $L_{\text{ph}}(\text{H})$ . A gradual increase of  $L_{\text{Min}}$  towards high  $T_{\text{h}}$  reflects a gradual decrease in  $L_{\text{ph}}(\text{H})$ , because a lower *number* of higher energy photons gives the same luminosity in  $\text{erg s}^{-1}$ .

Figure 6 thus demonstrates that the high quantity of the  $EM$  constrains  $L_{\text{Min}} > L_{\text{Edd}}$  for the temperatures given by model SEDs. It also shows that the parameters of the SSS, as derived from the X-ray-data models ( $T_{\text{h}} \sim 8 - 10 \times 10^5 \text{ K}$ ,  $L_{\text{h}} \lesssim L_{\text{Edd}}$ , Sect. 4.1), are not consistent with the observed amount of nebular emission. The values of  $EM$  require



$L_{\text{Min}}(8 - 10 \times 10^5 \text{ K}) = 2 - 7 L_{\text{Edd}}$  (see the intersection of the gray array with the dashed lines in Fig. 6). In other words,  $L_{\text{h}}$  and  $T_{\text{h}}$  obtained from the X-ray-data fits are not capable of producing the observed nebular emission. The  $EM$  of the thermal plasma thus represents a critical parameter in estimating the lower limit of the SSS luminosity.

In addition, a fraction of the ionizing photons can escape the star without being converted into the nebular radiation, and also the measured  $EM$  represents a lower limit of what was originally created by ionizations, because we observe only the optically thin part of the nebula. Under these circumstances the flux of ionizing photons, originally emitted by the star, is larger than that given by the equilibrium condition. This implies

$$L_{\text{h}} > L_{\text{Min}} > L_{\text{Edd}}. \quad (8)$$

(see Appendix A of Paper II in detail). In this way the large value of the  $EM$  justifies independently the WD's super-Eddington luminosity derived from the multiwavelength model SEDs, even during the SSS phase.

#### 4.4. The nature of the plateau phase

The plateau phase in the LC developed approximately between day 40 and 80 after the optical maximum, and is coincident with the SSS phase (Hachisu et al. , 2007). Figure 2 shows that the optical  $UBVRI$  region is dominated by the nebular continuum during this phase. A relatively slow decrease of the optical light thus reflects a relatively slow decrease in the  $EM$ . The variation in the  $EM$  follows solely that in the luminosity, because it is a function of the rate of  $L_{\text{ph}}$  photons. As a result, the slow decrease in the luminosity during the SSS phase causes a relevant decrease in the  $EM$ , which causes only a slow fading in the optical brightness, indicated in the LC as the *plateau phase* (see Fig. 1). Therefore, the cessation of the hydrogen burning around day 80, which stops the strong SSS phase (Hachisu et al. , 2007), ends also the plateau phase in the LC, because of a significant reduction of the WD's luminosity, i.e. production of the  $L_{\text{ph}}$  photons. Model SEDs beyond the SSS phase confirm this conclusion (Table 2, Fig. 3, Sect. 4.6).

Finally, I note that the *nebular* nature of the optical continuum during the SSS phase contradicts modelling the plateau phase in the LC with the *blackbody* radiation produced by a large disk irradiated by the WD photosphere as proposed by Hachisu et al. (2006).

#### 4.5. The growing mass of the WD due to its outbursts

The WD luminosity and the mass liberated during the burning phase ( $\sim 80$  days) allow us to estimate the amount of hydrogen burnt, and thus the mass added to the WD surface during the outburst,  $M_{\text{add}}^{\text{burnt}}$ . The prime energy source is the fusion of four protons that produces one helium atom. The mass difference between the input fuel and the output ash reveals that 0.7% of the mass of the original protons

is converted into energy, released in the form of gamma rays and neutrinos. This means that one gram of hydrogen can generate energy of  $\eta = 0.007 \times c^2 \sim 6.3 \times 10^{18} \text{ erg g}^{-1}$  (details of the hydrogen burning efficiency can be found in Mitalas , 1989). To estimate  $M_{\text{add}}^{\text{burnt}}$  I will assume that the energy generated by the thermonuclear fusion balances just the observed luminosity and the energy required to lift off the mass,  $\Delta M_{\text{wind}}$ , expelled via the wind, i.e.

$$M_{\text{add}}^{\text{burnt}} = 0.993 \mu \left( \frac{L_{\text{h}} \Delta t}{\eta} + \frac{GM_{\text{WD}} \Delta M_{\text{wind}}}{\eta R_{\text{WD}}} \right), \quad (9)$$

where  $\mu \sim 1.4$  is the mean molecular weight and  $\Delta t = 80$  days.

Modelling the broad  $H\alpha$  wings from the beginning of the eruption (day 1.38) and from the SSS phase (day 57) (see Skopal et al. , 2008), and the evolution in the line profiles along the outburst (e.g. Iijima , 2009; Banerjee et al. , 2009), suggested the mass loss rate via the wind at  $\approx 10^{-4} M_{\odot} \text{ yr}^{-1}$  for the first 10 days, and  $\approx 10^{-5} M_{\odot} \text{ yr}^{-1}$  during the following 70 days until the end of the hydrogen burning phase. Thus, the mass ejected from the accumulated WD envelope can be roughly estimated to  $\Delta M_{\text{wind}} \approx 10/365 \times 10^{-4} + 70/365 \times 10^{-5} = 4.6 \times 10^{-6} M_{\odot}$ . This value is a factor of  $\sim 1.6$  larger than that estimated by Hachisu et al. (2007). However, they assumed that the wind from the WD stopped already at the beginning of the SSS phase.

Assuming constant  $L_{\text{h}} \sim 1 \times 10^{40} \text{ erg s}^{-1}$  (Table 2), using parameters of a high-mass WD and  $\Delta t$  and  $\Delta M_{\text{wind}}$  as above, Eq. (9) yields  $M_{\text{add}}^{\text{burnt}} \sim 8 \times 10^{-6} M_{\odot}$  for  $d = 1.6 \text{ kpc}$ . For the outburst's recurrence time of 20 years, the WD mass in RS Oph is thus growing at an average rate of  $\dot{M}_{\text{WD}} \sim 4 \times 10^{-7} (d/1.6 \text{ kpc})^2 M_{\odot} \text{ yr}^{-1}$ . However, a certain fraction of the WD material can be dredged up and mixed into the ejecta due to the TNR. This effect can decrease the  $M_{\text{add}}^{\text{burnt}}$  mass and thus also its growing rate. Modelling the supersoft X-ray and visual LCs, Hachisu et al. (2007) derived  $\dot{M}_{\text{WD}} \sim 1 \times 10^{-7} M_{\odot} \text{ yr}^{-1}$ .

#### 4.6. Evolution beyond the SSS phase

Following the plateau phase in the LC (day  $\gtrsim 80$ ), both the stellar radiation from the WD and the nebular radiation were decreasing (Table 2, Sect. 3.2). A relatively strong contribution from the nebula (in both the continuum and lines), as measured around the middle of the monotonic decline, (day 93, Fig. 3) implied that the WD still emitted a large flux of ionizing photons at the rate  $\gtrsim 3 \times 10^{47} \text{ s}^{-1}$ .

During the post-outburst minimum (day 253, Fig. 3), the WD photosphere became markedly cooler ( $T_{\text{h}} \sim 25000 \text{ K}$ ) and larger ( $R_{\text{h}}^{\text{eff}} \sim 1 R_{\odot}$ ). The nebular contribution was negligible. As a result, the corresponding SED showed a minimum at the optical (see the figure). This effect was transient, because the following cooling of the hot component (i.e. the WD photosphere and the disk-like material surrounding it) caused filling-in the optical during the quiescent phase ( $\gtrsim 1$  year after the outburst).

During the quiescence, the flat UV/optical SED satisfied radiation produced by a large ( $R_{\text{disk}} > 10 R_{\odot}$ ) optically thick accretion disk (day 614, Fig. 3). In addition, the pronounced features of the iron curtain in the *IUE* spectra constrain the presence of the veiling material located at/behind the outer rim of the disk, and extended vertically from its plane, so to cause the observed absorptions. This naturally explains a significant depression of the X-ray luminosity indicated during the quiescent phase (Osborne et al. , 2011, and references therein). These properties imply that the disk-like formation in RS Oph is not geometrically thin as accretion disks in CVs. However, the satisfactory model SED with Eq. (2) suggests that the warm pseudophotosphere in RS Oph is also given by an ansamble of contributions radiating at different temperatures (probably along its projection to the sky).

The luminosity of the disk ( $(280 - 510)/\cos(i) L_{\odot}$ , Table 2) corresponds to an accretion rate of  $\dot{M}_{\text{acc}}(Q) = (1.6 - 3.0) \times 10^{-7} M_{\odot} \text{ yr}^{-1}$  for  $\alpha = 0.5$  (Starrfield et al. , 1988),  $M_{\text{WD}} \sim 1.3 M_{\odot}$ ,  $R_{\text{WD}} \sim 0.004 R_{\odot}$  and  $i = 50^{\circ}$  (Nauenberg , 1972; Yaron et al. , 2005; Brandi et al. , 2009). This implies that the high mass WD in RS Oph is accreting just below the stable burning limit (e.g. Shen and Bildsten , 2007; Wolf et al. , 2013). During the 20 years of quiescence the WD accumulates the mass of  $m_{\text{acc}}(Q) = (3.2 - 6.0) \times 10^{-6} M_{\odot}$ , which is sufficient to ignite a new outburst (see Eq. (10)).

Finally, according to the above-mentioned disk properties, the parameters  $L_{\text{h}}$  and  $\dot{M}_{\text{acc}}(Q)$  can be a factor of  $1/\cos(i)$  lower, but also can be somewhat larger, because a fraction of the radiation from the inner parts of the disk in the direction of poles cannot be detected (see Sect. 5.3.6 of Skopal , 2005). However, values of  $L_{\text{h}}$  and  $T_{\text{h}}$  from our model SED are consistent with those estimated by Dobrzycka et al. (1996), who classified the hot component in RS Oph during quiescence as a B-type shell star.

#### 4.7. On the accretion and ejection in RS Oph

Recently, Schaefer (2009) discussed in detail the accretion process in RS Oph, and concluded that wind accretion fails to provide enough mass to the WD required for an eruption. Therefore he assumed that the giant in RS Oph fills its Roche lobe, and placed the system to the distance of  $4.3 \pm 0.7 \text{ kpc}$ . However, this assumption is not consistent with the model SED of the red giant in RS Oph.

The large luminosity of the giant for the distance of 4.3 kpc,  $L_{\text{g}} = 690 (4.3/1.6 \text{ kpc})^2 \sim 5000 L_{\odot}$  (see Sect. 3.1 of Paper II), is not compatible with its small mass  $\mathcal{M}_{\text{g}} = 0.68 - 0.8 M_{\odot}$  (Brandi et al. , 2009) and the effective temperature  $T_{\text{eff}} = 3800 - 4200 \text{ K}$  (Paper II). Note that both  $\mathcal{M}_{\text{g}}$  and  $T_{\text{eff}}$  are distance independent. According to the current calibration of (super)giants (see Cox , 2000) and/or evolutionary models for single stars (e.g. de Loore & Doom , 1992), such stellar parameters are not consistent with any normal star.

Accordingly, the giant in RS Oph cannot fill its Roche

lobe, and thus the required high accretion rate cannot be a result of a standard Roche lobe overflow (see Sect. 4.7.3).

##### 4.7.1. On the origin of the massive nebula

The huge amount of the emitting mass,  $M^{\text{neb}} \gtrsim 10^{-4} (d/1.6 \text{ kpc})^{5/2} M_{\odot}$ , which surrounds the binary, persists in the system until the end of the hydrogen burning phase (Sect. 4.3.1). The presence of a significant amount of CSM in the system is also consistent with the high value of  $N_{\text{H}}$  during the whole SSS phase, which is by a factor of  $\sim 3$  larger than the interstellar value. Does this emitting CSM in RS Oph come from the accreted WD envelope? The answer is *no*. If this were the case, then the pressure at the base of the envelope,

$$P_{\text{base}} = G \frac{M_{\text{WD}} M_{\text{env}}}{4\pi R_{\text{WD}}^4}, \quad (10)$$

would be  $\sim 10^{21} \text{ dyne cm}^{-2}$  for parameters of a high-mass WD, which exceeds significantly the critical value,  $P_{\text{crit}} \approx 10^{19} \text{ dyne cm}^{-2}$ , required to ignite a TNR (e.g. Yaron et al. , 2005). This would also imply an unrealistically high average accretion rate ( $\dot{M}_{\text{acc}} \sim M_{\text{env}}/P_{\text{rec}} \sim 10^{-5} M_{\odot} \text{ yr}^{-1}$ ). Nevertheless, RS Oph ejected a fraction of the accreted mass, as was proved by extremely broad emission lines, observed at the beginning of its outburst (Buil , 2006; Tarasova , 2009; Iijima , 2009). In such a case the nuclear energy,  $E_{\text{nuc}}$ , has to be larger than the gravitational potential energy of the central WD, to lift a mass  $m_{\text{ej}}$  outside the system. This leads to a condition

$$m_{\text{ej}} < \frac{R_{\text{WD}}}{GM_{\text{WD}}} E_{\text{nuc}}, \quad (11)$$

where  $E_{\text{nuc}} = L_{\text{h}} \Delta t$  and  $m_{\text{ej}}$  is the mass released during the time  $\Delta t$ . Parameters,  $L_{\text{h}} \sim 10^{40} \text{ erg s}^{-1}$ ,  $\Delta t = 54 \text{ days}$ ,  $M_{\text{WD}} \sim 1.3 M_{\odot}$  and  $R_{\text{WD}} \sim 0.004 R_{\odot}$  (see above) yield  $m_{\text{ej}} < 4 \times 10^{-5} M_{\odot}$ . So, the emitting mass of  $\gtrsim 10^{-4} (d/1.6 \text{ kpc})^{5/2} M_{\odot}$ , as measured on day 54, could not be ejected from the WD surface.

Therefore, the large amount of mass, emitting during the RS Oph outbursts, has to have its origin outside the accreted envelope, most probably in a large disk encompassing the WD.

##### 4.7.2. Evidence for a disk around the WD

(i) During first  $\sim 30$  days after the explosion, a bipolar jet-like collimated outflow was indicated by the satellite components to the main cores of hydrogen line profiles (Skopal et al. , 2008; Banerjee et al. , 2009). Later, directly seen in the 43 GHz image (Sokoloski et al. , 2008). This indicates the presence of a disk, because jets require an accretion disk (e.g. Livio , 1997).

(ii) Photometric flickering variability became to be measurable shortly after the outburst, at day 117 (Zamanov et al. , 2006) and later on, increasing in the amplitude, through the whole period between outbursts (Dobrzycka et al. , 1996; Worters et al. , 2007; Hric et al. , 2008). It is believed that flickering originates from accretion onto a WD,

and thus its source can be located within the accretion disk (e.g. Bruch , 1992).

(iii) A pronounced double-peak structure in the H $\alpha$  profile was observed between nova eruptions (Zamanov et al. , 2005; Brandi et al. , 2009). After the 2006 outburst, a signature of this type of the profile was first measured on day 200 (2006, August 31) by Iijima (2009). The origin of the double-peak profile of hydrogen Balmer lines observed in symbiotic stars is often connected with an accretion disk (e.g. Robinson et al. , 1994).

(iv) The flux distribution from the UV to near-IR, during quiescent phase, could be modelled directly by the radiation from a large optically thick accretion disk ( $R_{\text{disk}} > 10 R_{\odot}$ , Sects. 3.2 and 4.6, Fig. 3). Assuming a typical average density in the disk  $\log(\rho) \approx -7$  in  $\text{g cm}^{-3}$ , the mass of the disk can be as high as  $\approx 10^{-4} M_{\odot}$ . It is of interest to note that the SED of RS Oph from quiescence is very similar to that of classical symbiotic stars during active phases, which requires a disk-like formation around the WD (e.g. Figs. 4, 5, 6, 27 of Skopal , 2005).

#### 4.7.3. On the accretion mechanism

The mass added on the WD surface due to hydrogen burning and the mass ejected during the outburst represent a minimum to the material accreted by the WD,  $m_{\text{acc}} \sim M_{\text{add}}^{\text{burnt}} + \Delta M_{\text{wind}} = 1.26 \times 10^{-5} M_{\odot}$  (Sect. 4.5). The high quantity of  $m_{\text{acc}}$  constrains the average accretion rate to  $\dot{M}_{\text{acc}} \equiv m_{\text{acc}}/P_{\text{rec}} \sim 6.3 \times 10^{-7} M_{\odot} \text{ yr}^{-1}$  for  $P_{\text{rec}} = 20$  years. During quiescence, the matter from the disk is accreted at  $\sim 2.3 \times 10^{-7} M_{\odot} \text{ yr}^{-1}$  (Sect. 4.6), which implies enhanced accretion during the 80-day burning phase to  $\sim 3.6 \times 10^{-5} M_{\odot} \text{ yr}^{-1}$  to balance the average accretion between outbursts. Such a high accretion rate during the outburst could be realized through the disk, as indicated by the presence of jets (Sect. 4.7.2).

The final problem in reconstructing the picture of the RS Oph outburst is to identify the source of material, which feeds the WD at the required rate. Comparison of the giant's luminosity in RS Oph (Sect. 3.1 of Paper II) with those in other symbiotic stars, suggests a wind mass loss rate from the giant,  $\dot{M}_{\text{giant,wind}} \sim 10^{-7} M_{\odot} \text{ yr}^{-1}$  (see Fig. 24 in Skopal , 2005). If the efficiency of the accretion process from the wind is (in maximum) of 10% (Nagae et al. , 2004), then the required  $\dot{M}_{\text{acc}} \gg 0.1 \times \dot{M}_{\text{giant,wind}}$ , which shows that the giant itself is not capable of supplying the necessary material to the WD in a standard wind accretion regime (see Schaefer , 2009, in detail). In connection with this problem, I will consider two possibilities.

(i) The only vital source of material for the accretion is the large amount of emitting CSM indicated during the hydrogen burning phase (Sect. 4.3.1). The relatively fast re-creation of the large disk in the system (see Sect. 4.6, Fig. 3) suggests that this material has to return back to the binary, where it enhances the accretion onto the WD. Observationally, this process is indicated directly by the A-type absorption lines, whose radial velocities indicate a

movement of absorbing material towards the binary at a velocity of  $\gtrsim 5 \text{ km s}^{-1}$  (see Fig. 3 and Table 2 of Brandi et al. , 2009).

In this case, when the accretion from the giant's wind is neglected, the large accretion rate from the disk-like reservoir of material implies a gradual decrease of the disk's mass and thus accretion. As a result, the recurrence time of the outbursts will extend, the growing of the WD mass will decelerate, and thus prolong the time, when the WD mass will reach the Chandrasekhar limit. The extending period (9, 18 and 21 years) between the most recent 4 explosions (1958, 1967, 1985 and 2006) supports this case. Accordingly, the next outburst should occur beyond 2027.

(ii) The primary source of the material powering the outburst is the wind from the giant. In this case the wind has to be compressed to the equatorial plane to fill in continuously the disk, and thus to keep the accretion rate at the required level. As a result, outbursts of RS Oph should be rather periodic, lasting for a long time, until the WD reach its limiting mass. In this case, the next explosion can occur even prior to 2027.

A possibility of a very effective mass transfer mode in binaries containing an evolved star – wind Roche-lobe overflow – was recently suggested by Mohamed and Podsiadlowski (2007). This mode can be in the effect, when the acceleration zone of the wind extends to the Roche lobe (see Fig. 1 of Abate et al. , 2013). Then, the wind of the giant is focused towards the orbital plane and in particular towards the WD, which then accretes at a significantly larger rate than from the spherically symmetric wind (Mohamed and Podsiadlowski , 2007; de Val-Borro et al. , 2009). A relatively small Roche-lobe radius of the giant in RS Oph,  $R_{\text{L,g}} \sim 2 \times R_{\text{g}}$  (see Paper II), is in favour of this case. Another possibility how to compress the wind from a star to the equatorial plane is the rotation of the central star (Bjorkman and Cassinelli , 1993). Zamanov and Stoyanov (2012) found that giants in symbiotic stars rotate with a mean  $v \sin(i) \sim 8 \text{ km s}^{-1}$ . Using this value and other characteristic parameters of the giant's wind in symbiotic stars (e.g.  $\dot{M}_{\text{giant,wind}} \sim 10^{-7} M_{\odot} \text{ yr}^{-1}$  as above and terminal velocity of 20–40  $\text{ km s}^{-1}$ ), the wind compression at the orbital plane and a distance of 2–3 A.U. from the wind source yields  $\dot{M}_{\text{giant,wind}} \gtrsim 10^{-6} M_{\odot} \text{ yr}^{-1}$  (Cariková and Skopal, in preparation). Such a high mass-loss rate should be capable of feeding the disk with a few times  $10^{-7} M_{\odot} \text{ yr}^{-1}$ .

## 5. Summary

In this paper I investigated the 14 Å to 37  $\mu\text{m}$  continuum radiation emitted by the recurrent symbiotic nova RS Oph during its SSS phase and the following transition to quiescence. For this purpose I used the method of multiwavelength modelling of the SED (see Paper I). Particularly, I disentangled the composite continuum at the beginning (day 40), middle (day 54) and the end (day 67) of the stable SSS phase, and during the final decline (day 93), the

post-outburst minimum (day 253) and the quiescence (day 614). During the SSS phase, the model SEDs revealed the presence of a very strong stellar as well as nebular component of radiation in the spectrum. The former was emitted by the burning WD, while the latter represents a fraction of its radiation reprocessed by the thermal nebula. During the transition to quiescence, both components were decreasing and during quiescence the SED satisfied radiation produced by a large ( $R_{\text{disk}} > 10 R_{\odot}$ ) optically thick accretion disk. The model SEDs are depicted in Figs. 2 and 3 and the corresponding physical parameters are found in Table 2. The main results of this paper can be summarized as follows.

- (i) *The stellar* component of radiation can be reproduced by that of a blackbody with an average effective radius  $R_{\text{h}}^{\text{eff}} \sim 0.23(d/1.6 \text{ kpc}) R_{\odot}$ , radiating at the temperature  $T_{\text{h}} \sim 490\,000 \text{ K}$ . This yields a luminosity  $L_{\text{h}} \sim 10^{40}(d/1.6 \text{ kpc})^2 \text{ erg s}^{-1}$ , which exceeds the Eddington luminosity by a factor of  $\sim 60$ . The X-ray fluxes were attenuated by the b-f absorptions corresponding to the total neutral hydrogen column density  $N_{\text{H}} \sim 7 \times 10^{21} \text{ cm}^{-2}$ , which exceeds the interstellar value by a factor of  $\sim 3$ . This reflects a significant additional attenuation by the CSM (Sect. 3.1, Fig. 2, Table 2). *The nebular* component of radiation dominated the spectrum from the mid-UV to longer wavelengths. It was characterized with an electron temperature  $T_{\text{e}} \sim 30\,000 \text{ K}$  and a large emission measure,  $EM \sim 2.2 \times 10^{61}(d/1.6 \text{ kpc})^2 \text{ cm}^{-3}$ . It was present in the spectrum throughout the whole SSS phase (Fig. 2, Table 2). *The radiation from the giant* was described in Paper II. Here, an additional argument that the giant underfills its Roche lobe is found in Sect. 4.7.
- (ii) The parameters of the SSS, as determined by the multiwavelength modelling the global SED, are very different from those obtained by fitting only the X-ray data. However, the X-ray-data models do not match the UV fluxes at all (Sect. 4.1, Fig. 4). Such a difference is given by the well known mutual dependence between the parameters  $L_{\text{h}}$ ,  $N_{\text{H}}$  and  $T_{\text{h}}$ , which allows to obtain a wide scale of solutions in fitting only the X-ray data (see Sect. 4.1 of Paper I). Therefore, the authors selected that satisfying the current theoretical predictions (e.g.  $L_{\text{h}} \lesssim L_{\text{Edd}}$  during the SSS phase).
- (iii) The super-Eddington luminosity during the SSS phase is independently supported by the high quantity of the nebular emission, which represents a fraction of the WD radiation reprocessed by the thermal nebula (Sect. 4.3.2, Fig. 6, Eq. (8)).
- (iv) The plateau phase in the LC is caused by a slow fading of the nebular radiation that dominates the optical. As the nebula was fed by the WD radiation, the cessation of the hydrogen burning around day 80, which stops the SSS phase, ends also the plateau phase in the LC (Sect. 4.4).
- (v) The large value of the  $EM$ , the volume and the flux of the emitting region as well as the strong flux in the  $\text{H}\alpha$

line correspond to a high mass of the nebular emitting material,  $M^{\text{neb}} = (1.6 \pm 0.5) \times 10^{-4}(d/1.6 \text{ kpc})^{5/2} M_{\odot}$  (Sect. 4.3.1). It has its origin outside the accreted envelope, in a large disk encompassing the WD (Sect. 4.7.1).

- (vi) The WD's luminosity and the energy required to lift off the mass from the WD during the burning phase correspond to the mass added on the WD surface due to hydrogen burning,  $M_{\text{add}}^{\text{burnt}} \sim 8 \times 10^{-6}(d/1.6 \text{ kpc})^2 M_{\odot}$ . For the outburst's recurrence time of 20 years, the WD mass in RS Oph is thus growing at an average rate of  $\dot{M}_{\text{WD}} \sim 4 \times 10^{-7}(d/1.6 \text{ kpc})^2 M_{\odot} \text{ yr}^{-1}$  (Sect. 4.5).
- (vii) The mass accreted by the WD between outbursts,  $m_{\text{acc}} \sim 1.26 \times 10^{-5} M_{\odot}$ , constrains the average accretion rate  $\dot{M}_{\text{acc}} \sim 6.3 \times 10^{-7} M_{\odot} \text{ yr}^{-1}$  (Sect. 4.7.3).
- (viii) During quiescence, the model SED requires an average accretion from the disk,  $\dot{M}_{\text{acc}}(Q) \sim 2.3 \times 10^{-7} M_{\odot} \text{ yr}^{-1}$ , which implies that the WD in RS Oph is accreting just below the stable burning limit. During the 20 years of quiescence, the WD thus accumulates the mass of  $m_{\text{acc}}(Q) \sim 4.6 \times 10^{-6} M_{\odot}$ , which is sufficient to ignite a new explosion (Sect. 4.6).
- (ix) During the 80-day burning phase, the accretion from the disk has to be enhanced to  $\sim 3.6 \times 10^{-5} M_{\odot} \text{ yr}^{-1}$  (Sect. 4.7.3). Such a high transient accretion rate is also signalized by the transient presence of jets (Sect. 4.7.2). It can be thus responsible for the super-Eddington luminosity during the whole hydrogen burning phase.
- (x) If the wind from the giant is *not* sufficient to feed the WD at the required rate, the accretion has to be realized from a disk-like reservoir of mass in the system. During the burning phase, the massive nebula can represent such the reservoir of the mass (Sects. 4.3.1 and 4.7.1). During the quiescent phase, the presence of a large and massive disk is indicated by the model SED (Sect. 4.7.2, point (iv)). In this case, the time between the outbursts will extend. The next outburst should occur beyond 2027, according to timing of the last 4 well observed explosions (1958, 1967, 1985, 2006, > 2027; Sect. 4.7.3, point (i)).
- (xi) If the primary source of the high accretion rate is the wind from the giant, then it has to be focused towards the orbital plane to fill in continuously the disk. Then, the next explosion can occur prior to 2027 (Sect. 4.7.3, point (ii)).

The solution of the multiwavelength modelling the global SED of the recurrent symbiotic nova RS Oph suggests that the mass transfer and accretion via the wind from the evolved star onto its compact companion in a wide binary must be more effective than the currently accepted view.

## Acknowledgments

I thank the anonymous referee for constructive comments. I am grateful to Horst Drechsel for a discussion to the early version of this work and all arrangements during my visits at the Astronomisches Institut der Universität Erlangen-Nürnberg in Bamberg (2008, 2010 and 2012). I thank Manfred Hanke for providing me the recent cross-sections for the X-ray absorption model and some advice about treatment the X-ray data. Nye Evans is thanked for providing me the *Spitzer* spectra of his original PID 270 proposal in a table form.

This work is in part based on observations obtained with *XMM-Newton*, an ESA science mission with instruments and contributions directly funded by ESA Member States and NASA. This research has also made use of data obtained from the *Chandra* X-ray observatory operated for NASA by the Smithsonian Astrophysical Observatory. This work profited from enormous effort of other astronomers, who gathered a large amount of multivavelength observations throughout the very wide wavelength range.

Finally, a partial support of this research was realized through a grant of Alexander von Humboldt foundation No. SLA/1039115 and a grant of the the Slovak Academy of Sciences, VEGA No. 2/0002/13.

## References

- Abate, C., Pols, O.R., Izzard, R.G., Mohamed, S.S., de Mink, S. E., 2013. *A&A* 552, A26.
- Banerjee, D.P.K., Das, R.K. Ashok, N.M., 2009. *MNRAS* 399, 357.
- Bjorkman, J.E., Cassinelli, J.P., 1993, *ApJ* 409, 429.
- Bode, M.F., O'Brien, T.J., Osborne, J.P., et al., 2006. *ApJ* 652, 629.
- Brandi, E., Quiroga, C., Mikolajewska, J., Ferrer, O.E., García, L.G., 2009. *A&A* 497, 815.
- Bruch, A., 1992. *A&A* 266, 237.
- Buil, Ch., 2006. CBET No. 403.
- Cox, A. N.: 2000, *Allen's Astrophysical Quantities*. AIP Press, New York
- de Loore, C. W. H., Doom, C., 1992. *Structure and Evolution of Single and Binary Stars*. Kluwer Acad. Publ., Dordrecht
- de Val-Borro, M., Karovska, M., Sasselov, D., 2009. *ApJ* 700, 1148
- Dobrzycka, D., Kenyon, S. J., Milone, A. A. E., 1996. *AJ* 111, 414
- Evans, A., Callus, C. M. Albinson, J. S., Whitelock, W. A., Glass, I. S., Carter, B., Roberts, G., 1988. *MNRAS* 234, 755
- Evans, A., Woodward, C. E., Helton, L. A., Gehrz, R. D., Lynch, D. K., Rudy, R. J., Russell, R. W., Kerr, T., 2007. *ApJ* 663, L29
- Eyres, S. P. S., O'Brien, T. J., Beswick, R., Muxlow, T. W. B., Anupama, G. C., Kantharia, N. G., Bode, M. F., Gawroski, M. P., 2009. *MNRAS* 395, 1533
- Gurzadyan, G. A., 1997. *The Physics and Dynamics of Planetary Nebulae*. Springer-Verlag, Berlin
- Hachisu, I., Kato, M., Kiyota, S., Kubotera, K., Maehara, H., Nakajima, K., Ishii, Y., Kamada, M., 2006. *ApJ* 651, L141
- Hachisu, I., Kato, M., Luna G. J. M., 2007. *ApJ* 659, L153
- Hric, L., Kundra, E., Niarchos, P., Manimanis, V. N., Likos, A., Gális, R., 2008. in Evans A., Bode M. F., O'Brien T. J., Darnley M. J., eds, *ASP Conf. Ser.* 401, *RS Ophiuchi (2006) and the Recurrent Nova Phenomenon*. ASP, San Francisco, p. 215
- Iben, I., Tutukov, A. V., 1996. *ApJS* 105, 145
- Iijima, T., 2009. *A&A* 505, 287
- Kwok, S., 2000. *The Origin and Evolution of Planetary Nebulae*. Cambridge University Press, Cambridge
- Livio, M., 1997. in Wickramashinge D. T., Bicknell G. V., Ferrario L., eds, *ASP Conf. Ser.* 121, *Accretion Phenomena and Related Outflows*. ASP, San Francisco, p. 845
- Mitalas, R., 1989. *ApJ* 338, 308
- Mohamed, S., Podsiadlowski, P., 2007. in 15th European Workshop on White Dwarfs, eds. R. Napiwotzki, & M. R. Burleigh, *ASP Conf. Ser.*, 372, ASP, San Francisco, p. 397
- Nagae, T., Oka, K., Matsuda, T., Fujiwara, H., Hachisu, I., Boffin, H. M. J., 2004. *A&A* 419, 335
- Narumi, H., Hirose, K., Kanai, K., et al., 2006. *IAU Circ.* 8671
- Nauenberg, M., 1972. *ApJ* 175, 417
- Nelson, T., Orio, M., Cassinelli, J. P., Leibowitz, E., Mucciarelli, P., 2008. *ApJ* 673, 1067
- Ness, J.-U., Starrfield, S., Beardmore, A. P., Bode, M. F., Drake, J. J., Evans, A., Gehrz, R. D., Goad, M. R., 2007. *ApJ* 665, 1334
- Ness, J.-U., Drake, J. J., Starrfield, S., et al., 2009. *AJ* 137, 3414
- O'Brien, T., Bode, M. F., Porcas, R. W., Muxlow, T. W. B., Eyres, S. P. S., Beswick, R. J., Garrington, S. T., Davis, R. J., Evans, A., 2006. *Nature* 442, 279
- Osborne, J., Page, K., Beardmore, A., Goad, M., Bode, M. F., O'Brien, T., Schwarz, G., Starrfield, S., 2006. *Astron. Tel.* 838, 1
- Osborne, J. P., Page, K. L., Beardmore, A. P., et al., 2011. *ApJ* 727:124 (10pp)
- Osterbrock, D. E., 1989. *Astrophysics of Gaseous Nebulae and Active Galactic Nuclei*. W. H. Freeman and Company Press, San Francisco
- Rauch, T., 2003. *A&A* 403, 709
- Robinson, K., Bode, M. F., Skopal, A., Ivison, R. J., Meaburn, J., 1994. *MNRAS* 269, 1
- Rupen, M. P., Mioduszewski, A. J., Sokoloski, J. L., 2008. *ApJ* 688, 559
- Schaefer, B. E., 2009. *ApJ* 697, 721
- Shen, K. J., Bildsten, L., 2007. *ApJ* 660, 1444
- Sekeráš, M., & Skopal, A., 2012. *MNRAS* 427, 979
- Skopal, A., 2005. *A&A* 440, 995
- Skopal, A., 2007. *New. Astron.* 12, 597

- Skopal, A., 2015a. *New. Astron.* (in press; arXiv:1401.1848, Paper I)
- Skopal, A., 2015b. *New. Astron.* (in press; arXiv:1402.6126, Paper II)
- Skopal, A., Pribulla T., Buil Ch., Vittone A., Errico, L., 2008. in Evans A., Bode M. F., O'Brien T. J., Darnley M. J., eds, *ASP Conf. Ser. 401, RS Ophiuchi (2006) and the Recurrent Nova Phenomenon*. ASP, San Francisco, p. 227
- Skopal, A., Pribulla, T., Budaj, J., Vittone, A. A., Errico, L., Wolf, M., Otsuka, M., Chrastina, M., Mikulášek, Z., 2009. *ApJ* 690, 1222
- Sokoloski, J. L., Luna, G. J. M., Mukai, K., Kenyon, S. J., 2006. *Nature* 442, 276
- Sokoloski, J. L., Rupen, M. P., Mioduszewski, A. J., 2008. *ApJ* 685, L137
- Starrfield, S., Sparks, W. M., Shaviv, G., 1988. *ApJ* 325, L35
- Tarasova, T. N., 2009. *Astronomy Reports* 53, 203
- Warner, B., 1995. *Cataclysmic Variable Stars* (New York: CUP), 43
- Wilms, J., Allen, A., McCray, R., 2000. *ApJ* 542, 914
- Wolf, W. M., Bildsten, L., Brooks, J., Paxton, B., 2013. *ApJ* 777, article id. 136, 15 pp.
- Worters, H. L., Eyres, S. P. S., Bromage, G. E., Osborne, J. P., 2007. *MNRAS* 379, 1557
- Zamanov, R. K., Bode, M. F., Tomov, N. A., Porter, J. M., 2005. *MNRAS* 363, L26
- Zamanov, R., Boër M., Le Coroller, H., Panov, K., 2006. *IBVS No. 5733*
- Zamanov, R.K., Stoyanov, K.A., 2012. *Bulgarian Astron. J.* 18-3, 41
- Yaron, O., Prialnik, D., Shara, M. M., Kovetz, A., 2005. *ApJ* 623, 398